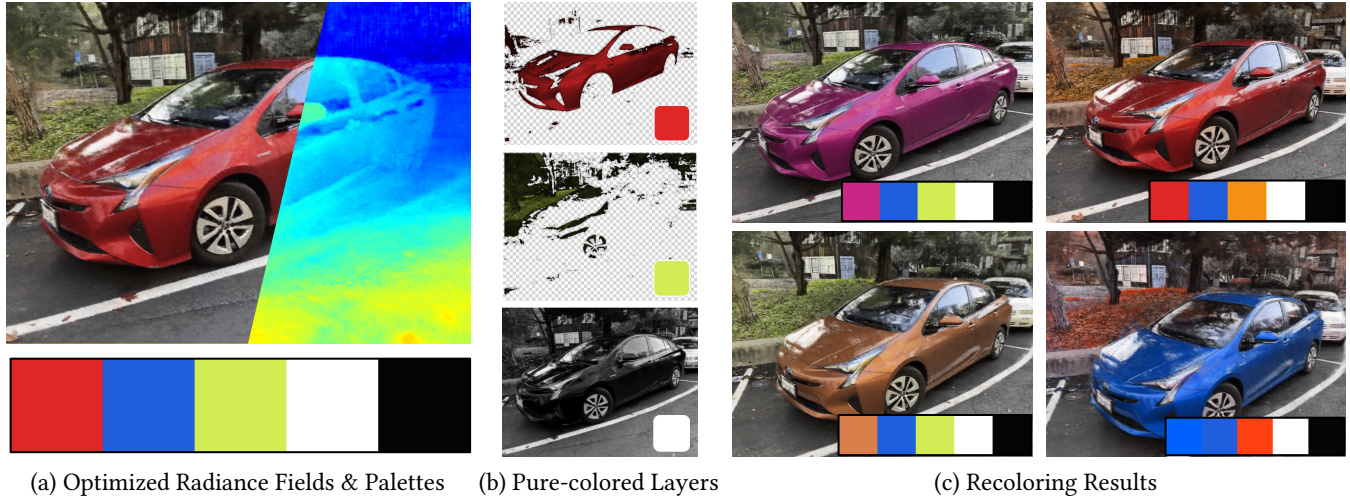


# RecolorNeRF: Layer Decomposed Radiance Fields for Efficient Color Editing of 3D Scenes

Bingchen Gong\*  
Yuehao Wang\*  
gongbingchen@gmail.com  
yhwang@link.cuhk.edu.hk  
The Chinese University of Hong Kong

Xiaoguang Han  
hanxiaoguang@cuhk.edu.cn  
The Chinese University of Hong Kong  
(Shenzhen)

Qi Dou  
qidou@cuhk.edu.hk  
The Chinese University of Hong Kong



**Figure 1:** Our method offers a user-friendly approach for recoloring 3D scenes. The scene is represented as a radiance field that is layer-decomposed and jointly optimized with an associated palette. Each color in the palette corresponds to a pure-colored layer. This design enables users to alter the color of each layer independently, producing high-fidelity recoloring results.

## ABSTRACT

Radiance fields have gradually become a main representation of media. Although its appearance editing has been studied, how to achieve view-consistent recoloring in an efficient manner is still under explored. We present RecolorNeRF, a novel user-friendly color editing approach for the neural radiance fields. Our key idea is to decompose the scene into a set of pure-colored layers, forming a palette. By this means, color manipulation can be conducted by altering the color components of the palette directly. To support efficient palette-based editing, the color of each layer needs to be as representative as possible. In the end, the problem is formulated as an optimization problem, where the layers and their blending weights are jointly optimized with the NeRF itself. Extensive experiments show that our jointly-optimized layer decomposition can be

\*Both authors contributed equally. Corresponding email to: gongbingchen@gmail.com

Permission to make digital or hard copies of all or part of this work for personal or classroom use is granted without fee provided that copies are not made or distributed for profit or commercial advantage and that copies bear this notice and the full citation on the first page. Copyrights for components of this work owned by others than the author(s) must be honored. Abstracting with credit is permitted. To copy otherwise, or republish, to post on servers or to redistribute to lists, requires prior specific permission and/or a fee. Request permissions from [permissions@acm.org](https://www.acm.org/permissions).

MM '23, October 29–November 3, 2023, Ottawa, ON, Canada

© 2023 Copyright held by the owner/author(s). Publication rights licensed to ACM.

ACM ISBN 979-8-4007-0108-5/23/10...\$15.00

<https://doi.org/10.1145/3581783.3611957>

used against multiple backbones and produce photo-realistic recolored novel-view renderings. We demonstrate that RecolorNeRF outperforms baseline methods both quantitatively and qualitatively for color editing even in complex real-world scenes. Our code and more results are available at <https://sites.google.com/view/recolornef>.

## CCS CONCEPTS

• **Computing methodologies** → **Reconstruction**; *Image-based rendering*; *Volumetric models*.

## KEYWORDS

radiance fields, recoloring, visual editing, neural rendering, palettes

## ACM Reference Format:

Bingchen Gong, Yuehao Wang, Xiaoguang Han, and Qi Dou. 2023. RecolorNeRF: Layer Decomposed Radiance Fields for Efficient Color Editing of 3D Scenes. In *Proceedings of the 31st ACM International Conference on Multimedia (MM '23)*, October 29–November 3, 2023, Ottawa, ON, Canada. ACM, New York, NY, USA, 17 pages. <https://doi.org/10.1145/3581783.3611957>

## 1 INTRODUCTION

Neural radiance fields (NeRF) have been proven to be a powerful representation of 3D scenes, which likely become a next-generation media form in the future, analogous to images and videos. To this end, supporting editing in such a new representation is critical.

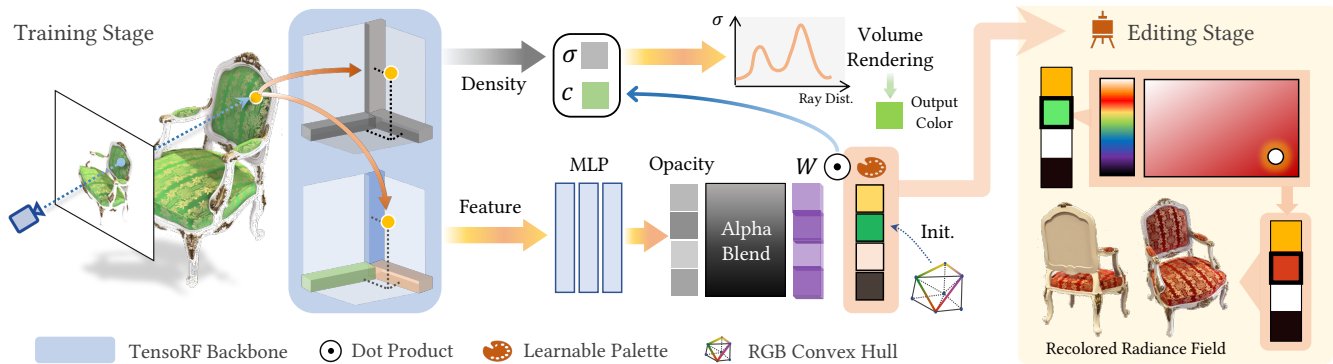


**Figure 2: Overview of our method.** During the training stage, the TensorRF [7] backbone and the learnable palette will be optimized to represent the color of any query point through alpha compositing over the learned palette. In the editing stage, users can simply replace a color in the palette with a new one to recolor the entire radiance field.

Very recently, several works on this topic have emerged, exploring editable NeRF in respect of scene composition [46, 56], geometry deformation [24, 29, 53, 55], appearance editing [15, 25, 54], style transfer [9, 11, 41, 57] etc. Recoloring is a sort of appearance editing that typically entails resetting a scene’s precise color tones for improvement or correction. It is a crucial process in the creation of both artistic and cinematic works. For example, using recoloring, the red car in Fig. 1 may be colored blue while maintaining photorealism.

Among all existing approaches to recoloring an image, palette-based color editing (PCE) [1, 50, 58] stands out due to its most intuitive and efficient user interaction. PCE first extracts a palette of representative colors from the image. Each color corresponds to a pure-colored layer. The image will be decomposed as a blending of the layers by solving the weight of each palette item. After that, we can simply alter the palette to precisely edit the image’s colors, such as tuning green layers to recolor grass and leaves in a “forest” image.

In this paper, we propose a novel method, RecolorNeRF, to conduct photo-realistic PCE on NeRF representations, which to our knowledge is the first attempt using a learnable palette for layer-wise decomposition of 3D scenes. Although [47] has performed NeRF recoloring based on palettes, its rendering results are compromised by its lossy posterization. Another possible approach to adapting PCE to NeRF is to first extract palettes from the pixels of all input images, using the heuristic method in [45], and then separately conduct layer decomposition and color editing for each novel view rendered from a pre-trained NeRF model. Despite being straightforward to implement, this solution suffers from exhausted per-view decomposition, poor view inconsistency, and 3D-agnostic palette extraction.

To address the aforementioned issues, our key idea is to optimize the palette, the layer decomposition, and the volumetric radiance fields in a unified framework. To deal with complicated scenes, we follow [40, 45] to use “over” composition as the imaging formulation. Specifically, the appearance of each point in a 3D scene is represented by an alpha blending of a set of ordered pure-colored layers, which form a palette for editing. To achieve this, we model the layer opacity as a volumetric alpha field for each layer. Our proposed approach also includes the first trial of geometric palette

optimization, which regularizes the palette to convexly span the color space of the 3D scene. Furthermore, in order to encourage the independence and representativeness of the learnable palette, sparsity of the blending weights is imposed through our novel soft sparsity norm and order-dependent weighting scheme.

Our RecolorNeRF can robustly decompose 3D scenes into multiple layers and enable diverse high-fidelity recoloring of complex 3D scenes in an efficient manner, without any restriction to backbone NeRF models, fine-tuning, and additional deep feature extraction. Our comparison experiments and a large-group user study also validate the superiority of our approach over other color editing methods for 3D scenes. In summary, our main contributions include:

- To our knowledge, we are the first attempt to perform photo-realistic palette-based color editing in NeRF representations via layer decomposition.
- We propose novel convex hull regularizations to jointly optimize the palette and the scene representation.
- Extensive recoloring experiments show that our carefully designed approach supports various complex scenes and different NeRF backbones.

## 2 RELATED WORK

### 2.1 NeRF Editing

Editing NeRFs is challenging due to their implicit scene representations. Existing works [24, 51, 54, 59, 60] support a few types of purely implicit editing on the target objects. NeRF-editing [55] extracts explicit meshes as a manipulable proxy and transfers the proxy movements back into the implicit representations. Approaches of [46, 56] present solutions to entity placement and scene composition in NeRF-represented scenes. NVDiffRec [29] extracts editable BRDF materials by disentangling 3D geometry and lighting effects from multi-view captures. EditNeRF [24] and CodeNeRF [54] are the recent NeRF models that encode simple objects’ shape and appearance into interpolative latent code. HDR-NeRF [15] and RawNeRF [25] use linear raw images as input rather than the post-processed ones, allowing controllable tone mapping during view synthesis. CLIP-NeRF [49] and DFFs [18] support text prompt or exemplar image-guided editing by leveraging the joint vision-language embedding of the CLIP model [38]. UPST-NeRF [9], INS [11] and ARF [57] propose different style transferring schemes and stylize NeRF



**Figure 3: Gallery of our color editing results. The first image of each row is the reference before editing along with the beneath optimized palette. The other 3 images showcase 3 examples of color editing with the corresponding edited palettes.**

models into reference images. NeRFEditor [41] encodes novel-view images into the hidden space of StyleGAN and enables interactive style editing on NeRF models.

Most of the above methods supporting style and appearance editing adopt additional encoders to extract high-level appearance code, while none of them decomposes the implicit representations in color space and endows intrinsic physical meanings to the decomposition. In contrast, our method can facilitate photo-realistic editing on both complex scenes and single objects without extra semantic-level features. The editing mode of our approach is more controllable and flexible, featuring precise color tuning and user-designed palettes. During the preparation of this paper, we noticed that there is a concurrent work PaletteNeRF [19] which also supports palette-based editing of NeRF models. Our method is different from theirs mainly in that we tend to decompose scenes into sparser layers using alpha blending, jointly optimize palettes and scene representations via more concise modeling, and allow the users to control the composition order of layers against a tailored palette. We include a result comparison between our method and PaletteNeRF in our supplementary materials to highlight the differences.

## 2.2 Color Editing

Color editing on images is a long-standing problem and has been well-studied in many scenarios. The challenge of color editing mainly lies in the extraction of editable color patterns. Failure of

sorting out color patterns will cause the so-called “color pollution” issue, which implies color edits upon different targets are mixed up and produces contamination-like artifacts. Many approaches exploit user guidance in pattern extraction by drawing colored scribbles or coarse spatial markers. Such approaches aim to recolor the meaningful patterns in the image by propagating the desired color through the user’s brushwork. Various algorithms [2, 8, 20, 22, 34, 52] are designed to propagate the user-specified edits. The problem is often formulated as an energy minimization problem, where Euclidean distance or diffusion distance in feature space is adopted to measure the affinity among pixels. Drawing scribbles demands higher costs on the user side than reference-based or palette-based methods since users need to provide meaningful guidance both in spatial and color domains. Color transfer is another form of reference-based color editing, in which the source image absorbs the color patterns of another reference image. Early color transfer methods [35, 39] change the colors of the source image based on the color distribution of a reference image. Reinhard et al. [39] performs color transfer by matching the means and standard deviations of the source color distribution to the reference one. Pitie et al. [35] explore a color mapping between source and reference images via color probability density function transferring. Histograms are widely used to represent the color distributions of images. Delon et al. [10] propose a color transfer method that segments the color histogram to construct palettes and warp the source color to the target by referring to the palettes.

## 2.3 Palette-based Recoloring

Palette-based recoloring methods allow users to tune color components by modifying a finite set of colors, which is a trade-off solution between user control and recoloring capability. A palette is a succinct representation that can describe the color scheme of an image. The most essential step in palette-based recoloring is palette extraction. Some previous methods fit predictive models of human palette preference and generate perceptual palettes from input images [5, 12, 21, 30]. A more straightforward approach to extract palettes for color editing is using the k-means algorithm to cluster the image colors in RGB space [6, 58]. This captures the most prominent colors in the image. Another palette-based approach consists of computing and simplifying the convex hull that encloses all the color samples [45]. This yields more “primary” palettes that better represent the color gamut of the image. Once we have the palette extracted, we can use it to represent the colors in the image by decomposing the image into layers, where each layer corresponds to an importance map of a palette color. The layer decomposition performs as a reverse procedure of layer composition. Several previous methods are proposed to composite the layers simply via weighted additive mixing [1, 44, 50, 58]. One most common alpha blending operator “over” composite is also used in recent methods to composite order-dependent layers [40, 43, 45]. Our method uses alpha blending, allows users control of palette order, and facilitates sparser layer decomposition.

## 3 PRELIMINARIES

### 3.1 Neural Radiance Fields

Neural Radiance Fields are introduced by [27] as a differentiable rendering model that can be trained to synthesize photo-realistic novel views by taking multi-view images as the input. Ordinary NeRFs can be regarded as an MLP function that maps coordinates into color and density values in the form of  $F_{\Theta}(\mathbf{x}, \mathbf{d}) \rightarrow (\mathbf{c}, \sigma)$ , where  $\Theta$  represents network parameters,  $\mathbf{x} = (x, y, z)$  is the 3D coordinates of a sampled point,  $\mathbf{d} = (\theta, \phi)$  is the view-in direction,  $\mathbf{c}$  is the predicted color, and  $\sigma$  is the predicted density. With this scene representation, the rendered color  $\hat{\mathbf{C}}(\mathbf{r}(t))$  of the image pixel corresponding to the ray  $\mathbf{r}(t) = (\mathbf{o}, \mathbf{d})$  can be evaluated via volume rendering (Eq. 1), where  $M$  is the number of samples along  $\mathbf{r}(t)$ ,  $\Delta_j$  is the step length of the  $j$ -th sample,  $\tau_j$  can be seen as the probability that the ray can reach the  $j$ -th sample.

$$\hat{\mathbf{C}}(\mathbf{r}(t)) = \sum_{j=1}^M \tau_j \mathbf{c}_j, \tau_j = \exp\left(-\sum_{i=1}^{j-1} \sigma_i \Delta_i\right) \left(1 - \exp(-\sigma_j \Delta_j)\right) \quad (1)$$

Then, the scene representation can be optimized in a learning fashion via minimizing the photometric loss between the rendered color and the ground-truth color  $\mathbf{C}(\mathbf{r}(t))$  in input images (Eq. 2). Here  $\mathcal{B}$  is a batch of the training rays.

$$\mathcal{L}_{color} = \sum_{\mathbf{r}(t) \in \mathcal{B}} \|\hat{\mathbf{C}}(\mathbf{r}(t)) - \mathbf{C}(\mathbf{r}(t))\|_2^2 \quad (2)$$

There are also many variants of NeRFs. DirectVoxGO [42], Plenoxels [13], Instant-NGP [28], TensoRF [7], etc. accelerate training of radiance fields by converting the fully implicit scene representations into explicit feature grids with an implicit shading module

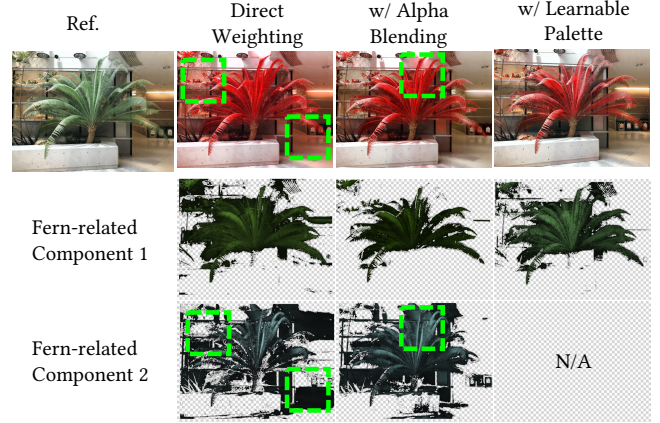


**Figure 4: Ablations on alpha blending and learnable palettes with the goal of recoloring a fern into red. The fern-related layers decomposed via Direct Weight, Alpha Blending and Alpha Blending with Learnable Palette are visualized.**

or spherical harmonics. In particular, TensoRF [7] factorizes the feature grids into compact low-rank tensor components, achieving considerable rendering quality, shorter training time, and smaller model size. Besides training acceleration, D-NeRF [37] and Nerfies [31] extend NeRF to dynamic scenes via modeling movements as 4D implicit motion fields. Furthermore, HyperNeRF [32] views each frame of dynamic scenes as a slice in a higher-dimensional latent space and manages to handle topology-varying movements.

### 3.2 Alpha Compositing

Alpha compositing, also called alpha blending, is a technique to order-dependently combine multiple image layers into a single image. Each image layer is associated with an alpha channel that is a gray-scale image of values among  $[0, 1]$  and specifies the per-pixel opacity of the layer. The blending operators are first introduced by [36]. A commonly-used one is defined as Eq. 3, where pixel color  $C_a$  with opacity  $\alpha_a$  is placed over pixel color  $C_b$  with opacity  $\alpha_b$  to composite new color  $C_o$  and opacity  $\alpha_o$ .

$$\alpha_o = \alpha_a + \alpha_b(1 - \alpha_a), C_o = \frac{C_a \alpha_a + C_b \alpha_b(1 - \alpha_a)}{\alpha_o} \quad (3)$$

To blend multiple image layers, we can recursively apply Eq. 3 to the upper and lower layers. In fact, Eq. 3 depicts a general painting operation. When the opacity of a pixel is 0, there is no overlay on the beneath pixels. While the opacity increases to 1, the pixel becomes opaque and gradually covers the underneath pixels. Our approach extends alpha compositing to 3D scenarios with differentiable properties and view-dependent effects.

## 4 RECOLORNERF

In this section, we describe our proposed method RecolorNeRF, including automatic layer decomposition via alpha blending activation and joint optimization of palettes and scene representations.

#### 4.1 Palette-based Layer Decomposition via Alpha Blending Activation

Suppose we have an ordered palette  $P = \{p_i \in [0, 1]^3\}_{i=1}^K$ , we aim to decompose a radiance field into  $K$  pure colored radiance layers, where the  $i$ th layer corresponds to the  $i$ th item of the palette. We define  $p_1$  as the color of the background layer and  $p_K$  as the color of the topmost layer. Our scene representation is modeled as Eq. 4.

$$F_{\Theta}(\mathbf{x}, \mathbf{d}) \rightarrow (\alpha_1, \alpha_2, \dots, \alpha_K, \sigma) \quad (4)$$

The model computes view-dependent opacity values  $\alpha_i(\mathbf{x}, \mathbf{d})$  for each layer. After retrieving opacity values from the model, we composite the radiance layers via alpha blending to yield the radiance field. By recursively applying Eq. 3 to the opacity fields  $\alpha_i(\mathbf{x}, \mathbf{d})$  and the palette  $P$ , we can obtain  $\mathbf{c}(\mathbf{x}, \mathbf{d})$  as Eq. 5:

$$\mathbf{c}(\mathbf{x}, \mathbf{d}) = p_K + \sum_{i=1}^{K-1} \left[ (p_i - p_{i+1}) \prod_{j=i+1}^{K-1} (1 - \alpha_j(\mathbf{x}, \mathbf{d})) \right] \quad (5)$$

The cumulative multiplication in Eq.5 will cause optimization numerically unstable. To better integrate alpha compositing into deep models as a stable differentiable function, we sort out coefficients of each  $p_i$  and transform them into logarithmic space:

$$\mathcal{T}(\alpha_i(\mathbf{x}, \mathbf{d})) = \begin{cases} \sum_{j=i+1}^K \log(1 - \alpha_j(\mathbf{x}, \mathbf{d})) & i = 1 \\ \log \alpha_i(\mathbf{x}, \mathbf{d}) + \sum_{j=i+1}^K \log(1 - \alpha_j(\mathbf{x}, \mathbf{d})) & 1 < i < K \\ \log(1 - \alpha_i(\mathbf{x}, \mathbf{d})) & i = K \end{cases} \quad (6)$$

We can show that  $\sum_{i=1}^K \exp[\mathcal{T}(\alpha_i(\mathbf{x}, \mathbf{d}))] = 1$ . Thereby we define an alpha blending activation  $\zeta(\cdot)$  as Eq. 7, which maps opacity to generalized barycentric coordinates. This alpha blending activation is differentiable and numerically stable, compared with the cumulative multiplication in Eq. 5. Consequently, the radiance field can be seen as a convex combination of the palette  $p_i \in P$ :

$$\mathbf{c}(\mathbf{x}, \mathbf{d}) = \sum_{i=1}^K \zeta(\alpha_i(\mathbf{x}, \mathbf{d})) p_i, \text{ where } \zeta(\alpha) = \exp[\mathcal{T}(\alpha)] \quad (7)$$

Since the geometry of the scene is independent of the opacity values, we separate the parameters of the geometry and appearance models. To achieve this, we adopt TensorRF [7] as our backbone, which simultaneously enables fast model training. The overview pipeline of our method is present in Fig. 2.

#### 4.2 Palette Learning

The key to successful layer decomposition is an optimal palette  $P$  that can express the entire color space of the 3D scene. For 2D images, Tan et al. [45] propose to model a palette as convex hull vertices of the pixel colors. In this way, any pixel color can be uniquely expressed as a convex combination of the palette colors. Inspired by this, we choose to formulate  $P$  as a set of convex hull vertices, encompassing the entire color space of the scene. Note that our alpha blending activation can coherently support this formulation since it naturally yields convex combinations of the palette. However, directly using the convex hull vertices as palettes is not feasible for user editing due to the convex hull will have thousands of vertices. Tan et al. [44] design an iterative heuristic convex hull simplification algorithm for reducing the palette to a user-desired

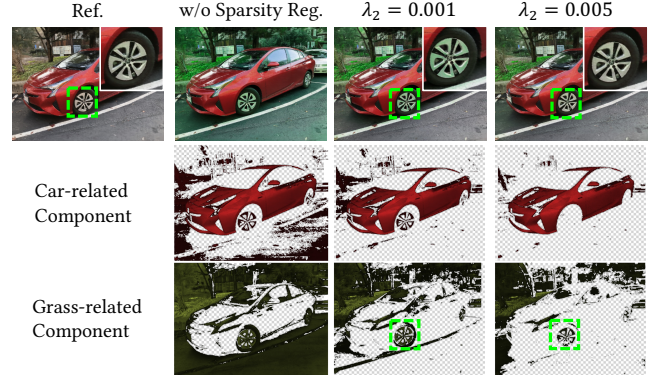


**Figure 5: Ablations of sparsity regularization with the goal of recoloring the background grass into greener. The component of foreground car and background grass are visualized.**

size. Our empirical study finds that palettes pre-computed from this heuristic approach lead to many failure cases of layer decomposition in 3D scenes since only the 2D image-level color distribution is exploited. In this regard, we incorporate learnable palettes into the optimization of 3D scene representation and layer decomposition, as a group of training parameters. In order to preserve the geometric properties of palettes, we propose novel *convex hull bounding* and *projection-based convex* regularizations, which jointly guide the optimization trajectory of the palette.

*Convex Hull Bounding Regularization.* The learnable palette  $P$  should not be unbounded, since  $P$  is a subset of  $[0, 1]^3$  at most. To further shrink the bound of palette colors, we build a bounding convex hull from all input images (Eq. 8).

$$U = \left\{ \sum_{c_j \in \mathcal{P}} \lambda_j c_j \mid \lambda_j \geq 0 \text{ for all } j \text{ and } \sum_j \lambda_j = 1 \right\} \quad (8)$$

where  $\mathcal{P}$  is the universal set of all pixel colors in all multi-view images. We employ this bounding convex hull to form a feasible region by penalizing out-of-bound palette colors. To achieve this, we first find a set  $S(U)$  of all simplices of the bounding convex hull  $U$ . Then, we regularize the Euclidean distance from palette color  $p_i$  to its closest point on the simplex facets  $s \in S(U)$ , if  $p_i \notin U$ . The described regularization term is given in Eq. 9.

$$\mathcal{L}_{bd} = \sum_{i=1}^K \omega_{out} \mathbb{1}\{p_i \notin U\} \min_{s \in S(U)} \|p_i - \text{Nearest}(p_i|s)\|_2 \quad (9)$$

where  $\omega_{out}$  is the penalty strength,  $\text{Nearest}(p_i|s)$  finds closest point on the simplex facet  $s$  to the color  $p_i$ , and  $\mathbb{1}\{p_i \notin U\}$  denotes the indicator of  $p_i \notin U$ .

*Projection-based Convex Regularization.* In addition to bounding the range of palette colors, the palette is expected to maintain its convexity. Our solution is to project the palette colors to the vertices of the bounding convex hull. In essence, this projection-based optimization strategy imposes a constraint  $P \subset \text{HullVertices}(U)$ . Specifically, the regularizer in Eq. 10 is proposed to turn palette

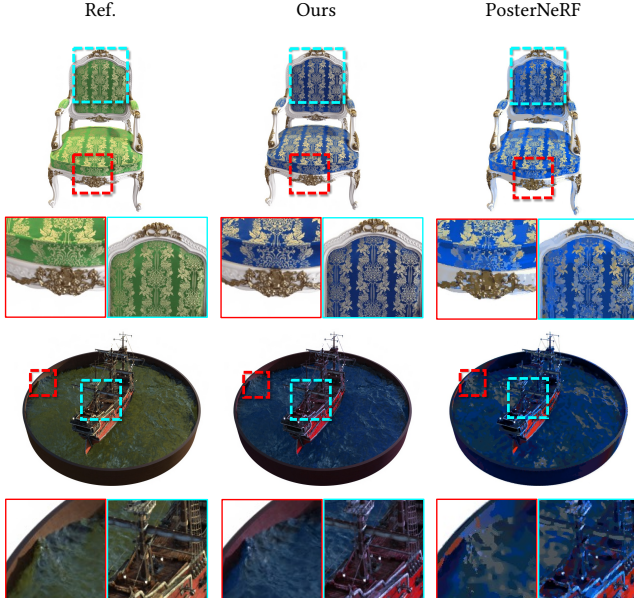


**Figure 6: Comparisons of our method and PosterNeRF on Synthetic NeRF dataset. In the first case, we aim to recolor the green chair into the blue without change of the yellow patterns. In the second case, we aim to recolor the orange ship into red and tune the water surface into blue.**

gradients towards the vertices of  $U$ .

$$\mathcal{L}_{proj} = \sum_{i=1}^K \omega_{in} \mathbb{1}\{p_i \in U\} \min_{v \in \text{HullVertices}(U)} \|p_i - v\|_2 \quad (10)$$

Finally, we combine the two regularizations to  $\mathcal{L}_{hull} = \mathcal{L}_{bd} + \mathcal{L}_{proj}$ . In our implementation, we generally set  $\omega_{out} = 1$  and  $\omega_{in} = 0.001$  to enforce a strong out-of-bound penalty and slow down the projection to the bounding convex hull, in order to prevent palette colors from fast convergence to nearby sub-optimal vertices.

*Palette Initialization.* As learnable parameters, random initialization of the palette could work for most cases. However, a user-designed prior palette can further promote the editability of the scene. For instance, one may move his/her target edit layer to the top layer and drop undesired layers to the background, in accordance with the alpha blending property that the color of the upper layer relates to fewer areas/objects. To this end, we support a human-involved palette initialization strategy, where the user first inputs a prior palette with expected ordering, then our method jointly optimizes the input palette to attain better layer decomposition. We find prior palettes can facilitate our method to extract representative layers in more complex scenes.

### 4.3 Rendering and Optimization

The volumetric rendering with the alpha compositing for a training ray  $\mathbf{r}(t) = (\mathbf{o}, \mathbf{d})$  is given in Eq. 11.

$$\hat{\mathbf{C}}(\mathbf{r}(t)) = \sum_{j=1}^M \tau_j \sum_{i=1}^K \zeta(\alpha_i(\mathbf{x}_j, \mathbf{d})) p_i \quad (11)$$

Recall that  $M$  is the number of samples along the ray and  $\tau_j$  is the accumulated transmittance, as described in Eq. 1. The scene representation can be optimized by minimizing the squared errors between the rendered color and the ground truth color, as in Eq. 2. To encourage sparser layer decomposition, we add a *layer sparsity* regularization to the scene optimization.

*Layer Sparsity Regularization.* The sparsity of opacity fields is preferred during layer decomposition. Sparser weights of the palette indicate the palette is more representative and the decomposition is more complete. We first render a weighting map  $W_i(\mathbf{r}(t))$  for each layer to estimate palette components around occupied space:

$$W_i(\mathbf{r}(t)) = \sum_{j=1}^M \tau_j \zeta(\alpha_i(\mathbf{x}_j, \mathbf{d})) \quad (12)$$

Next, we aim to penalize the L0 norm of these components, i.e.,  $\| [W_1, \dots, W_K] \|_0$ . Since the L0 norm is not differentiable, we design a specialized soft counting norm (Eq. 13) based on the Sigmoid function to conduct the sparsity penalty.

$$h_0(\mathbf{W}) = \sum_{l=1}^K \exp\left(\frac{l}{K} - 1\right) \left[1 + \exp(-\eta W_l + \beta)\right]^{-1} \quad (13)$$

The first exponential term in  $h_0$  order-dependently re-scales the sparsity of different layers such that the upper layers gain more sparsity than the lower layers. The reciprocal term in  $h_0$  approximates the Heaviside function on  $[0, 1]$ , where  $\eta$  and  $\beta$  are sparsity strength hyper-parameters, controlling the step edge sharpness and counting threshold. In our implementation,  $\beta$  is constantly set to 6 and  $\eta$  is set to 24 or 48, depending on the scene’s complexity. In the end, the batch-wise sparsity regularization is written as Eq. 14.

$$\mathcal{L}_{sparsity} = \sum_{\mathbf{r}(t) \in \mathcal{B}} h_0([W_1(\mathbf{r}(t)), \dots, W_K(\mathbf{r}(t))]) \quad (14)$$

*Overall Loss.* The overall objective function of our joint optimization is the weighted sum of photometric reconstruction loss, palette regularization  $\mathcal{L}_{hull}$  and sparsity penalty  $\mathcal{L}_{sparsity}$ , defined as:

$$\mathcal{L} = \mathcal{L}_{color} + \lambda_1 \mathcal{L}_{hull} + \lambda_2 \mathcal{L}_{sparsity} \quad (15)$$

where  $\lambda_1 = 1$  and  $\lambda_2 = 0.001$  or  $0.005$  in our experiments.

*Recoloring.* Upon decomposing a scene into layers with a learned palette, RecolorNeRF enables user color manipulation via palette adjustment, allowing efficient editing of diverse color schemes with typically less than 10 palettes per scene through re-rendering.

## 5 EXPERIMENTAL RESULTS

### 5.1 Evaluation

*Datasets.* We evaluate our method on  $360^\circ$  synthetic objects (Synthetic NeRF [27] and Synthetic NSVF [23] datasets), forward-facing real-world scenes (LLFF [26]), and  $360^\circ$  real-world objects (Tank and Temples[17, 23]).

*Baselines.* We compare our method with 4 recent state-of-the-art image-level or NeRF-level color editing baselines. For image-level PCE, we apply Tan et al.’s approach [44] to NeRF rendering results. We consider 2 schemes for building palettes for novel views. 1) Each novel view admits an independent palette. We dub this scheme **NeRF + Image PCE**. 2) Novel views share a unified palette built

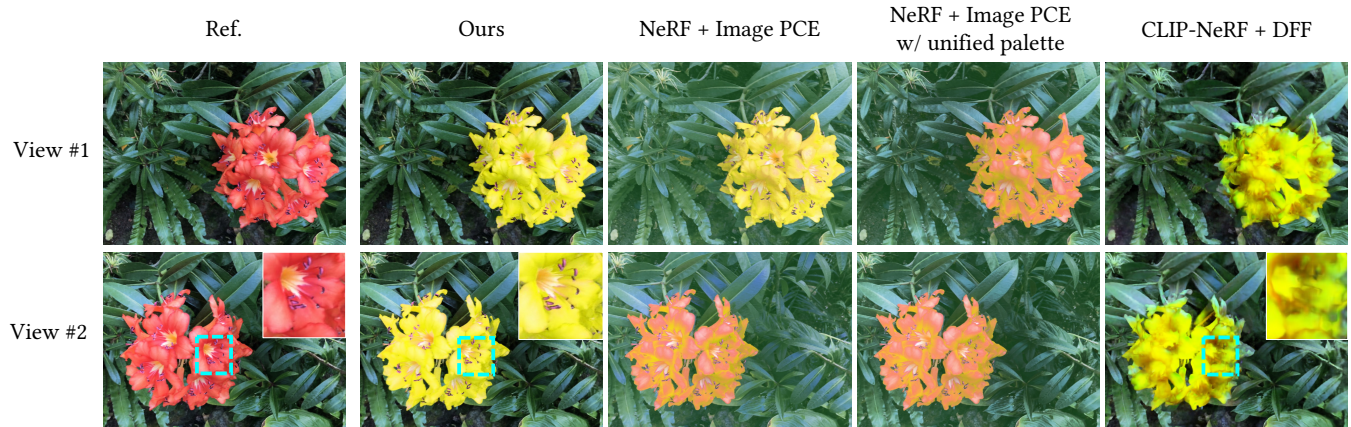


**Figure 7: Comparisons of our method, NeRF + Image PCE, NeRF + Image PCE w/ unified palette and CLIP-NeRF + DFF. We aim to recolor the red flower into yellow. For our method and PCE baselines, we replace red components with yellow to perform recoloring. For CLIP-NeRF + DFF, we fine-tune an optimized DFF model with text prompt ‘yellow flower’ and background filtered out.**

from all views’ pixels. We dub this one **NeRF + Image PCE w/ unified palette**. In addition to image-level editing, **PosterNeRF** [47] is included as a NeRF-level PCE baseline on the Synthetic NeRF datasets. We also compare with the recent text-driven scene editing method CLIP-NeRF [49]. To be precise, we use its follow-up implementation with distilled feature fields (DFF) [18], dubbed **CLIP-NeRF + DFF**.

*User Study.* To quantitatively evaluate recoloring performance from users’ aesthetic perspective, we conduct a user study to validate the advantage of our method. We first prepare 25 editing targets for various scenes (14 synthetic objects and 11 real-world scenes). Then, we accordingly generate recoloring results using our method and other baselines (only if the baseline supports the case). For each case, we ask respondents to select the most satisfied recoloring result that matches the editing target best. Our user study questionnaires are distributed online with randomized orders of questions and choices. Respondents are encouraged to spend at least 20 minutes completing the questionnaire. We collect 5081 valid ratings from 68 independent respondents. A visualization of the user study results is shown in Fig. 9. We can see that our method outperforms the other baselines both in real-world and synthetic scenes by a large margin. Especially for real-world scenes with complex color distributions, our method is much preferred. The overall results reflect our method is able to generate more aesthetic editing on various scenarios and possesses better recoloring capacity.

*Qualitative Comparison.* In qualitative evaluation, we visualize results from different methods and compare their rendering quality and recoloring capability. Fig. 6 exhibits the comparison results of our method versus PosterNeRF on the Synthetic NeRF datasets. From the close-ups, we can observe our method outperforms PosterNeRF both in rendering quality and recoloring. Our method can precisely extract editing patterns and recolor them without polluting other areas. In contrast, PosterNeRF blends the colors of editing areas and undesired areas. Fig. 7 compares our method with other 3 baselines in a forward-facing “flower” scene. We can observe that view consistency is not guaranteed by NeRF

+ Image PCE. Even if using a view-shared palette, NeRF + Image PCE w/ unified palette fails to recolor the red flower but mistakenly brightens the background leaves. CLIP-NeRF + DFF manages to change the color of the flower by text prompt. However, its rendering quality is compromised. Also, CLIP-NeRF + DFF is limited by the expressions of text prompts when it is difficult to describe editing targets in text.

## 5.2 Ablation Study

*Sparsity Regularization.* We do an ablation study to certify the effect of sparsity regularization. Fig. 5 visualizes layers of car and grass, decomposed under no sparsity regularization, weak sparsity regularization ( $\lambda_2 = 0.001$ ) and strong sparsity regularization ( $\lambda_2 = 0.001$ ), respectively. Without any regularization on sparsity, the grass component is dispersed in the entire background, leading to obvious color pollution when recolored into greener. By adding weak regularization on layer sparsity, the car layer and grass layer are separated out. Looking into the recoloring result, we can find slight color pollution occurs on the tire of the car. By imposing stronger sparsity regularization, the decomposition becomes more complete and further mitigates the color pollution.

*Alpha Blending with Learnable Palette.* To evaluate the effect of alpha blending, we replace the alpha blending with the direct weighting of the palette (named Direct Weighting). We also disable the learnable palettes to evaluate the effect of our palette learning. As shown in Fig. 4, we can see Direct Weighting scheme fails to completely decompose the foreground and the background even with our sparsity regularization. With this deficiency, recoloring the foreground will pollute the tones of the background. Alpha blending facilitates layer decomposition and alleviates the color pollution problem during recoloring. We owe this to the order-dependent formulation in the alpha blending. Furthermore, the learnable palette can further promote the separation of the background and foreground layers. In the shown case, the fern-related components are optimized to be merged. Thus, the green component becomes more representative, leading to better recoloring results.

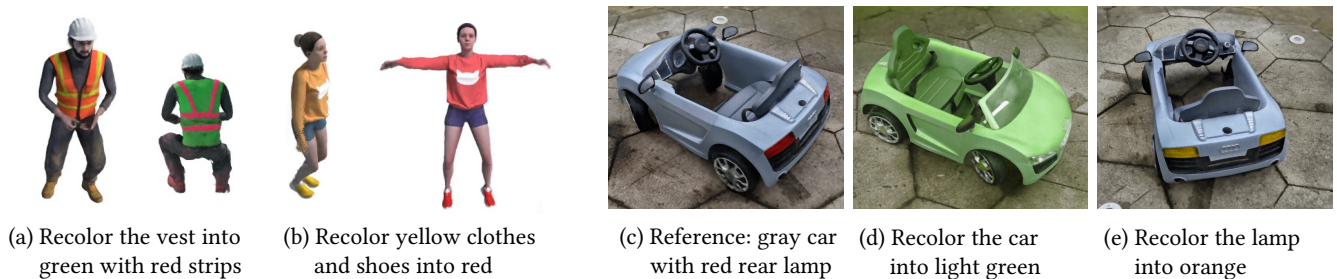


**Figure 8: Recoloring results of our method using D-NeRF [37] and Ref-NeRF [48] as backbones. (a) and (b) demonstrates recoloring of synthetic dynamic objects. (c) (d) and (e) showcase recoloring of real-world 360° scenes with metallic and translucent materials.**

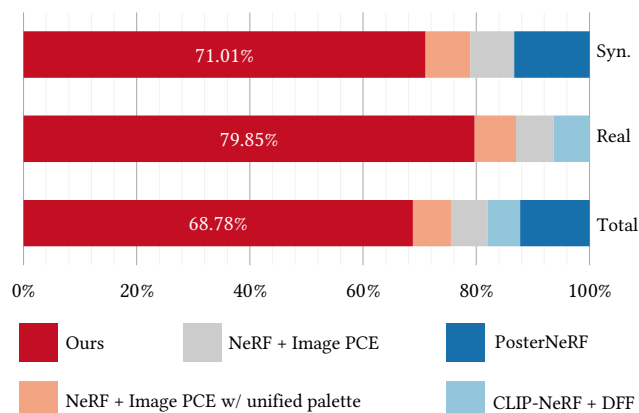


**Figure 9: User study statistics. Each color bar of a corresponding method indicates the user selection proportion among all questions that compare the results of the method. In the synthetic scenes, the proportion is 71.01%/7.91%/7.76%/13.33% from left to right. In the real-world scenes, the proportion from left to right is 79.85%/7.32%/6.66%/6.37%. In total, the proportion is 68.78%/6.86%/6.41%/6.58%/5.70%.**

*Synthesis Quality with Palette.* To assess the quality of our radiance field rendering using alpha blending and palettes, we compare photometric errors of our method and the original backbone TensorRF. The palettes in our model are initialized with 2 schemes: 1) user input and 2) automatic palette extraction via RGB-space hull simplification [45]. Table 1 reports the PSNR, SSIM, and LPIPS metrics. The user-customized palette scheme offers more controllable color editing, albeit with slightly lower performance. Our model initialized with automatically extracted palettes yields even better rendering results, further validating the effectiveness of alpha blending with palettes in view synthesis.

### 5.3 More Visual Results

We showcase the results of our RecolorNeRF in Fig. 3 and more in supplementary materials. Moreover, our approach can universally support other backbones. Fig. 8 shows the results of our approach with D-NeRF [37] and Ref-NeRF [48] backbones. This also illustrates the prospective applications of our method, e.g., virtual car repainting and digital clothes recoloring in online shopping.

**Table 1: Comparisons of novel view synthesis results between the original backbone and RecolorNeRF initialized with user-input palettes (user init.) and automatic palettes via hull simplification (auto init.), respectively.**

Models	PSNR $\uparrow$	SSIM $\uparrow$	LPIPS $\downarrow$
Original TensorRF	28.32 $\pm$ 5.21	0.852 $\pm$ 0.119	0.186 $\pm$ 0.129
Ours (user init.)	28.03 $\pm$ 4.87	0.843 $\pm$ 0.125	0.199 $\pm$ 0.138
Ours (auto init.)	28.76 $\pm$ 4.86	0.869 $\pm$ 0.111	0.169 $\pm$ 0.128

## 6 CONCLUSION

RecolorNeRF is an effective method to generate recolored photo-realistic novel views. We are the first to propose a method to decompose neural radiance fields into multiple pure-colored layers for recoloring. The decomposed layer are jointly optimized with a learnable palette to produce more disjoint decomposition and more representative colors in the palette. The layers are then stacked with alpha blending to generate color radiance and render the final photo-realistic images. Recoloring a scene is as simple as altering the color in palettes.

*Limitations.* The RecolorNeRF is only designed for overall color editing rather than instance-level editing. Since layer decomposition is merely based on colors, two different objects with similar colors will be decomposed into one layer. In this case, their color cannot be changed separately. Thus, one of the future improvements of RecolorNeRF is to incorporate semantics into layer decomposition.

## ACKNOWLEDGMENTS

This work was supported in part by Shenzhen Portion of Shenzhen-Hong Kong Science and Technology Innovation Cooperation Zone under HZQB-KCZYB-20200089, in part by Hong Kong Research Grants Council Project No. 24209223, in part by Science, Technology and Innovation Commission of Shenzhen Municipality Project No. SGDX20220530111201008, in part by NSFC-62172348, in part by Outstanding Young Fund of Guangdong Province with No. 2023B1515020055, in part by Shenzhen General Project with No. JCYJ20220530143604010, and in part by CCF-Tencent Open Research Fund.



## REFERENCES

- [1] Yağiz Aksoy, Tuğç Ozan Aydin, Aljoša Smolić, and Marc Pollefeys. 2017. Unmixing-Based Soft Color Segmentation for Image Manipulation. *ACM Trans. Graph.* 36, 4, Article 61c (jul 2017), 19 pages. <https://doi.org/10.1145/3072959.3002176>
- [2] Xiaobo An and Fabio Pellacini. 2008. AppProp: All-Pairs Appearance-Space Edit Propagation. *ACM Trans. Graph.* 27, 3 (aug 2008), 1–9. <https://doi.org/10.1145/1360612.1360639>
- [3] Jonathan T Barron, Ben Mildenhall, Matthew Tancik, Peter Hedman, Ricardo Martin-Brualla, and Pratul P Srinivasan. 2021. Mip-nerf: A multiscale representation for anti-aliasing neural radiance fields. In *Proceedings of the IEEE/CVF International Conference on Computer Vision*. 5855–5864.
- [4] Tim Brooks, Aleksander Holynski, and Alexei A Efros. 2023. Instructpix2pix: Learning to follow image editing instructions. In *Proceedings of the IEEE/CVF Conference on Computer Vision and Pattern Recognition*. 18392–18402.
- [5] Ying Cao, Antoni B. Chan, and Rynson W. H. Lau. 2017. Mining Probabilistic Color Palettes for Summarizing Color Use in Artwork Collections. In *SIGGRAPH Asia 2017 Symposium on Visualization (Bangkok, Thailand) (SA '17)*. Association for Computing Machinery, New York, NY, USA, Article 1, 8 pages. <https://doi.org/10.1145/3139295.3139296>
- [6] Huiwen Chang, Ohad Fried, Yiming Liu, Stephen DiVerdi, and Adam Finkelstein. 2015. Palette-Based Photo Recoloring. *ACM Trans. Graph.* 34, 4, Article 139 (jul 2015), 11 pages. <https://doi.org/10.1145/2766978>
- [7] Anpei Chen, Zexiang Xu, Andreas Geiger, Jingyi Yu, and Hao Su. 2022. TensorRF: Tensorial Radiance Fields. In *Computer Vision – ECCV 2022*, Shai Avidan, Gabriel Brostow, Moustapha Cissé, Giovanni Maria Farinella, and Tal Hassner (Eds.). Springer Nature Switzerland, Cham, 333–350.
- [8] Xiaowu Chen, Dongqing Zou, Qinqing Zhao, and Ping Tan. 2012. Manifold Preserving Edit Propagation. *ACM Trans. Graph.* 31, 6, Article 132 (nov 2012), 7 pages. <https://doi.org/10.1145/2366145.2366151>
- [9] Yaosen Chen, Qi Yuan, Zhiqiang Li, Yuegen Liu, Wei Wang, Chaoping Xie, Xuming Wen, and Qien Yu. 2022. UPST-NeRF: Universal Photorealistic Style Transfer of Neural Radiance Fields for 3D Scene. *arXiv preprint arXiv:2208.07059* (2022).
- [10] Julie Delon, Agnes Desolneux, Jose Luis Lisani, and Ana Belen Petro. 2005. Automatic color palette. In *IEEE International Conference on Image Processing 2005*, Vol. 2. II–706. <https://doi.org/10.1109/ICIP.2005.1530153>
- [11] Zhiwen Fan, Yifan Jiang, Peihao Wang, Xinyu Gong, Dejia Xu, and Zhangyang Wang. 2022. Unified Implicit Neural Stylization. In *Computer Vision – ECCV 2022*, Shai Avidan, Gabriel Brostow, Moustapha Cissé, Giovanni Maria Farinella, and Tal Hassner (Eds.). Springer Nature Switzerland, Cham, 636–654.
- [12] Zunlei Feng, Wolong Yuan, Chunli Fu, Jie Lei, and Mingli Song. 2018. Finding intrinsic color themes in images with human visual perception. *Neurocomputing* 273 (2018), 395–402. <https://doi.org/10.1016/j.neucom.2017.07.043>
- [13] Sara Fridovich-Keil, Alex Yu, Matthew Tancik, Qinhong Chen, Benjamin Recht, and Angjoo Kanazawa. 2022. Plenoxels: Radiance Fields Without Neural Networks. In *Proceedings of the IEEE/CVF Conference on Computer Vision and Pattern Recognition (CVPR)*. 5501–5510.
- [14] Ayaan Haque, Matthew Tancik, Alexei Efros, Aleksander Holynski, and Angjoo Kanazawa. 2023. Instruct-NeRF2NeRF: Editing 3D Scenes with Instructions. In *Proceedings of the IEEE/CVF International Conference on Computer Vision*.
- [15] Xin Huang, Qi Zhang, Ying Feng, Hongdong Li, Xuan Wang, and Qing Wang. 2022. HDR-NeRF: High Dynamic Range Neural Radiance Fields. In *Proceedings of the IEEE/CVF Conference on Computer Vision and Pattern Recognition (CVPR)*. 18398–18408.
- [16] Diederik P Kingma and Jimmy Ba. 2014. Adam: A method for stochastic optimization. *arXiv preprint arXiv:1412.6980* (2014).
- [17] Arno Knapitsch, Jaesik Park, Qian-Yi Zhou, and Vladlen Koltun. 2017. Tanks and Temples: Benchmarking Large-Scale Scene Reconstruction. *ACM Trans. Graph.* 36, 4, Article 78 (jul 2017), 13 pages. <https://doi.org/10.1145/3072959.3073599>
- [18] Sosuke Kobayashi, Eiichi Matsumoto, and Vincent Sitzmann. 2022. Decomposing NeRF for Editing via Feature Field Distillation. In *Advances in Neural Information Processing Systems*, S. Koyejo, S. Mohamed, A. Agarwal, D. Belgrave, K. Cho, and A. Oh (Eds.), Vol. 35. Curran Associates, Inc., 23311–23330. [https://proceedings.neurips.cc/paper\\_files/paper/2022/file/93f250215e4889119807b6fac3a57aec-Paper-Conference.pdf](https://proceedings.neurips.cc/paper_files/paper/2022/file/93f250215e4889119807b6fac3a57aec-Paper-Conference.pdf)
- [19] Zhengfei Kuang, Fujun Luan, Sai Bi, Zhixin Shu, Gordon Wetzstein, and Kalyan Sunkavalli. 2023. PaletteNeRF: Palette-Based Appearance Editing of Neural Radiance Fields. In *Proceedings of the IEEE/CVF Conference on Computer Vision and Pattern Recognition (CVPR)*. 20691–20700.
- [20] Anat Levin, Dani Lischinski, and Yair Weiss. 2004. Colorization Using Optimization. In *ACM SIGGRAPH 2004 Papers* (Los Angeles, California) (*SIGGRAPH '04*). Association for Computing Machinery, New York, NY, USA, 689–694. <https://doi.org/10.1145/1186562.1015780>
- [21] Sharon Lin and Pat Hanrahan. 2013. Modeling How People Extract Color Themes from Images. In *Proceedings of the SIGCHI Conference on Human Factors in Computing Systems* (Paris, France) (*CHI '13*). Association for Computing Machinery, New York, NY, USA, 3101–3110. <https://doi.org/10.1145/2470654.2466424>
- [22] Dani Lischinski, Zeev Farbman, Matt Uyttendaele, and Richard Szeliski. 2006. Interactive Local Adjustment of Tonal Values. *ACM Trans. Graph.* 25, 3 (jul 2006), 646–653. <https://doi.org/10.1145/1141911.1141936>
- [23] Lingjie Liu, Jiatao Gu, Kyaw Zaw Lin, Tat-Seng Chua, and Christian Theobalt. 2020. Neural Sparse Voxel Fields. In *Proceedings of the 34th International Conference on Neural Information Processing Systems (Vancouver, BC, Canada) (NIPS'20)*. Curran Associates Inc., Red Hook, NY, USA, Article 1313, 13 pages.
- [24] Steven Liu, Xiuming Zhang, Zhoutong Zhang, Richard Zhang, Jun-Yan Zhu, and Bryan Russell. 2021. Editing Conditional Radiance Fields. In *Proceedings of the IEEE/CVF International Conference on Computer Vision (ICCV)*. 5773–5783.
- [25] Ben Mildenhall, Peter Hedman, Ricardo Martin-Brualla, Pratul P. Srinivasan, and Jonathan T. Barron. 2022. NeRF in the Dark: High Dynamic Range View Synthesis From Noisy Raw Images. In *Proceedings of the IEEE/CVF Conference on Computer Vision and Pattern Recognition (CVPR)*. 16190–16199.
- [26] Ben Mildenhall, Pratul P. Srinivasan, Rodrigo Ortiz-Cayon, Nima Khademi Kalantari, Ravi Ramamoorthi, Ren Ng, and Abhishek Kar. 2019. Nical Light Field Fusion: Practical View Synthesis with Prescriptive Sampling Guidelines. *ACM Trans. Graph.* 38, 4, Article 29 (jul 2019), 14 pages. <https://doi.org/10.1145/3306346.3322980>
- [27] Ben Mildenhall, Pratul P. Srinivasan, Matthew Tancik, Jonathan T. Barron, Ravi Ramamoorthi, and Ren Ng. 2021. NeRF: Representing Scenes as Neural Radiance Fields for View Synthesis. *Commun. ACM* 65, 1 (dec 2021), 99–106. <https://doi.org/10.1145/3503250>
- [28] Thomas Müller, Alex Evans, Christoph Schied, and Alexander Keller. 2022. Instant Neural Graphics Primitives with a Multiresolution Hash Encoding. *ACM Trans. Graph.* 41, 4, Article 102 (jul 2022), 15 pages. <https://doi.org/10.1145/3528223.3530127>
- [29] Jacob Munkberg, Jon Hasselgren, Tianchang Shen, Jun Gao, Wenzheng Chen, Alex Evans, Thomas Müller, and Sanja Fidler. 2022. Extracting Triangular 3D Models, Materials, and Lighting From Images. In *Proceedings of the IEEE/CVF Conference on Computer Vision and Pattern Recognition (CVPR)*. 8280–8290.
- [30] Peter O'Donovan, Aseem Agarwala, and Aaron Hertzmann. 2011. Color Compatibility from Large Datasets. *ACM Trans. Graph.* 30, 4, Article 63 (jul 2011), 12 pages. <https://doi.org/10.1145/2010324.1964958>
- [31] Keunhong Park, Utkarsh Sinha, Jonathan T. Barron, Sofien Bouaziz, Dan B Goldman, Steven M. Seitz, and Ricardo Martin-Brualla. 2021. Nerfies: Deformable Neural Radiance Fields. In *Proceedings of the IEEE/CVF International Conference on Computer Vision (ICCV)*. 5865–5874.
- [32] Keunhong Park, Utkarsh Sinha, Peter Hedman, Jonathan T. Barron, Sofien Bouaziz, Dan B Goldman, Ricardo Martin-Brualla, and Steven M. Seitz. 2021. HyperNeRF: A Higher-Dimensional Representation for Topologically Varying Neural Radiance Fields. *ACM Trans. Graph.* 40, 6, Article 238 (dec 2021), 12 pages. <https://doi.org/10.1145/3478513.3480487>
- [33] Adam Paszke, Sam Gross, Francisco Massa, Adam Lerer, James Bradbury, Gregory Chanan, Trevor Killeen, Zeming Lin, Natalia Gimelshein, Luca Antiga, et al. 2019. Pytorch: An imperative style, high-performance deep learning library. *Advances in neural information processing systems* 32 (2019).
- [34] Fabio Pellacini and Jason Lawrence. 2007. AppWand: Editing Measured Materials Using Appearance-Driven Optimization. *ACM Trans. Graph.* 26, 3 (jul 2007), 54–es. <https://doi.org/10.1145/1276377.1276444>
- [35] Francois Pitié, Anil C Kokaram, and Rozenn Dahyot. 2005. N-dimensional probability density function transfer and its application to color transfer. In *Tenth IEEE International Conference on Computer Vision (ICCV'05) Volume 1*, Vol. 2. 1434–1439 Vol. 2. <https://doi.org/10.1109/ICCV.2005.166>
- [36] Thomas Porter and Tom Duff. 1984. Compositing Digital Images. In *Proceedings of the 11th Annual Conference on Computer Graphics and Interactive Techniques (SIGGRAPH '84)*. Association for Computing Machinery, New York, NY, USA, 253–259. <https://doi.org/10.1145/800031.808606>
- [37] Albert Pumarola, Enric Corona, Gerard Pons-Moll, and Francesc Moreno-Noguer. 2021. D-NeRF: Neural Radiance Fields for Dynamic Scenes. In *Proceedings of the IEEE/CVF Conference on Computer Vision and Pattern Recognition (CVPR)*. 10318–10327.
- [38] Alec Radford, Jong Wook Kim, Chris Hallacy, Aditya Ramesh, Gabriel Goh, Sandhini Agarwal, Girish Sastry, Amanda Askell, Pamela Mishkin, Jack Clark, Gretchen Krueger, and Ilya Sutskever. 2021. Learning Transferable Visual Models From Natural Language Supervision. In *Proceedings of the 38th International Conference on Machine Learning (Proceedings of Machine Learning Research, Vol. 139)*, Marina Meila and Tong Zhang (Eds.). PMLR, 8748–8763. <https://proceedings.mlr.press/v139/radford21a.html>
- [39] Erik Reinhard, Michael Adhikhmin, Bruce Gooch, and Peter Shirley. 2001. Color transfer between images. *IEEE Computer Graphics and Applications* 21, 5 (July 2001), 34–41. <https://doi.org/10.1109/38.946629>
- [40] Christian Richardt, Jorge Lopez-Moreno, Adrien Bousseau, Maneesh Agrawala, and George Drettakis. 2014. Vectorising Bitmaps into Semi-Transparent Gradient Layers. *Computer Graphics Forum* 33, 4 (2014), 11–19. <https://doi.org/10.1111/cgf.12408> arXiv:https://onlinelibrary.wiley.com/doi/pdf/10.1111/cgf.12408
- [41] Chunyi Sun, Yanbing Liu, Junlin Fan, and Stephen Gould. 2022. NeRFEditor: Differentiable Style Decomposition for Full 3D Scene Editing. *arXiv preprint arXiv:2212.03848* (2022).

- [42] Cheng Sun, Min Sun, and Hwann-Tzong Chen. 2022. Direct Voxel Grid Optimization: Super-Fast Convergence for Radiance Fields Reconstruction. In *Proceedings of the IEEE/CVF Conference on Computer Vision and Pattern Recognition (CVPR)*. 5459–5469.
- [43] Jianchao Tan, Marek Dvorník, Daniel Šýkora, and Yotam Gingold. 2015. Decomposing Time-Lapse Paintings into Layers. *ACM Trans. Graph.* 34, 4, Article 61 (jul 2015), 10 pages. <https://doi.org/10.1145/2766960>
- [44] Jianchao Tan, Jose Echevarria, and Yotam Gingold. 2018. Efficient Palette-Based Decomposition and Recoloring of Images via RGBXY-Space Geometry. *ACM Trans. Graph.* 37, 6, Article 262 (dec 2018), 10 pages. <https://doi.org/10.1145/3272127.3275054>
- [45] Jianchao Tan, Jyh-Ming Lien, and Yotam Gingold. 2016. Decomposing Images into Layers via RGB-Space Geometry. *ACM Trans. Graph.* 36, 1, Article 7 (nov 2016), 14 pages. <https://doi.org/10.1145/2988229>
- [46] Jiaxiang Tang, Xiaokang Chen, Jingbo Wang, and Gang Zeng. 2022. Compressible-composable NeRF via Rank-residual Decomposition. In *Advances in Neural Information Processing Systems*, S. Koyejo, S. Mohamed, A. Agarwal, D. Belgrave, K. Cho, and A. Oh (Eds.), Vol. 35. Curran Associates, Inc., 14798–14809. [https://proceedings.neurips.cc/paper\\_files/paper/2022/file/5ed5c3c846f684a54975ad7a2525199f-Paper-Conference.pdf](https://proceedings.neurips.cc/paper_files/paper/2022/file/5ed5c3c846f684a54975ad7a2525199f-Paper-Conference.pdf)
- [47] Kenji Tojo and Nobuyuki Umetani. 2022. Recolorable Posterization of Volumetric Radiance Fields Using Visibility-Weighted Palette Extraction. *Computer Graphics Forum* 41, 4 (2022), 149–160. <https://doi.org/10.1111/cgf.14594> arXiv:<https://onlinelibrary.wiley.com/doi/pdf/10.1111/cgf.14594>
- [48] Dor Verbin, Peter Hedman, Ben Mildenhall, Todd Zickler, Jonathan T. Barron, and Pratul P. Srinivasan. 2022. Ref-NeRF: Structured View-Dependent Appearance for Neural Radiance Fields. In *Proceedings of the IEEE/CVF Conference on Computer Vision and Pattern Recognition (CVPR)*. 5491–5500.
- [49] Can Wang, Menglei Chai, Mingming He, Dongdong Chen, and Jing Liao. 2022. CLIP-NeRF: Text-and-Image Driven Manipulation of Neural Radiance Fields. In *Proceedings of the IEEE/CVF Conference on Computer Vision and Pattern Recognition (CVPR)*. 3835–3844.
- [50] Yili Wang, Yifan Liu, and Kun Xu. 2019. An Improved Geometric Approach for Palette-based Image Decomposition and Recoloring. *Computer Graphics Forum* 38, 7 (2019), 11–22. <https://doi.org/10.1111/cgf.13812> arXiv:<https://onlinelibrary.wiley.com/doi/pdf/10.1111/cgf.13812>
- [51] Dejia Xu, Peihao Wang, Yifan Jiang, Zhiwen Fan, and Zhangyang Wang. 2022. Signal Processing for Implicit Neural Representations. In *Advances in Neural Information Processing Systems*, S. Koyejo, S. Mohamed, A. Agarwal, D. Belgrave, K. Cho, and A. Oh (Eds.), Vol. 35. Curran Associates, Inc., 13404–13418. [https://proceedings.neurips.cc/paper\\_files/paper/2022/file/575c450013d0e99e4b0ecf82bd1afaa4-Paper-Conference.pdf](https://proceedings.neurips.cc/paper_files/paper/2022/file/575c450013d0e99e4b0ecf82bd1afaa4-Paper-Conference.pdf)
- [52] Kun Xu, Yong Li, Tao Ju, Shi-Min Hu, and Tian-Qiang Liu. 2009. Efficient Affinity-Based Edit Propagation Using K-D Tree. *ACM Trans. Graph.* 28, 5 (dec 2009), 1–6. <https://doi.org/10.1145/1618452.1618464>
- [53] Tianhan Xu and Tatsuya Harada. 2022. Deforming Radiance Fields with Cages. In *Computer Vision – ECCV 2022*, Shai Avidan, Gabriel Brostow, Moustapha Cissé, Giovanni Maria Farinella, and Tal Hassner (Eds.). Springer Nature Switzerland, Cham, 159–175.
- [54] Bangbang Yang, Yinda Zhang, Yinghao Xu, Yijin Li, Han Zhou, Hujun Bao, Guofeng Zhang, and Zhaopeng Cui. 2021. Learning Object-Compositional Neural Radiance Field for Editable Scene Rendering. In *Proceedings of the IEEE/CVF International Conference on Computer Vision (ICCV)*. 13779–13788.
- [55] Yu-Jie Yuan, Yang-Tian Sun, Yu-Kun Lai, Yuwen Ma, Rongfei Jia, and Lin Gao. 2022. NeRF-Editing: Geometry Editing of Neural Radiance Fields. In *Proceedings of the IEEE/CVF Conference on Computer Vision and Pattern Recognition (CVPR)*. 18353–18364.
- [56] Jiakai Zhang, Xinhang Liu, Xinyi Ye, Fuqiang Zhao, Yanshun Zhang, Minye Wu, Yingliang Zhang, Lan Xu, and Jingyi Yu. 2021. Editable Free-Viewpoint Video Using a Layered Neural Representation. *ACM Trans. Graph.* 40, 4, Article 149 (jul 2021), 18 pages. <https://doi.org/10.1145/3450626.3459756>
- [57] Kai Zhang, Nick Kolkin, Sai Bi, Fuzun Luan, Zexiang Xu, Eli Shechtman, and Noah Snavely. 2022. ARF: Artistic Radiance Fields. In *Computer Vision – ECCV 2022*, Shai Avidan, Gabriel Brostow, Moustapha Cissé, Giovanni Maria Farinella, and Tal Hassner (Eds.). Springer Nature Switzerland, Cham, 717–733.
- [58] Qing Zhang, Chunxia Xiao, Hanqiu Sun, and Feng Tang. 2017. Palette-Based Image Recoloring Using Color Decomposition Optimization. *IEEE Transactions on Image Processing* 26, 4 (April 2017), 1952–1964. <https://doi.org/10.1109/TIP.2017.2671779>
- [59] Chengwei Zheng, Wenbin Lin, and Feng Xu. 2023. EditableNeRF: Editing Topologically Varying Neural Radiance Fields by Key Points. In *Proceedings of the IEEE/CVF Conference on Computer Vision and Pattern Recognition (CVPR)*. 8317–8327.
- [60] Yiyu Zhuang, Hao Zhu, Xusen Sun, and Xun Cao. 2022. MoFaNeRF: Morphable Facial Neural Radiance Field. In *Computer Vision – ECCV 2022*, Shai Avidan, Gabriel Brostow, Moustapha Cissé, Giovanni Maria Farinella, and Tal Hassner (Eds.). Springer Nature Switzerland, Cham, 268–285.

## A IMPLEMENTATION DETAILS

We implement our entire model and training pipeline with PyTorch [33]. Our implementation is based on TensorRF [7] without any customized CUDA kernels.

*TensorRF Backbone.* We utilize TensorRF-VM as our backbone for querying density and opacity values, which offers a more compact scene representation compared to pure grid-based representations [13, 42] and achieves faster training convergence than the original pure MLP-based representations [3, 27]. To disentangle the geometry and appearance of the scene, we construct separate density field  $\mathcal{T}_\sigma$  and opacity field  $\mathcal{T}_c$ . Specifically, TensorRF-VM factorizes the geometry of the 3D space as a sum of outer products of vectors and matrices, as shown in Eq. 16.

$$\mathcal{T}_\sigma = \sum_{m \in [3]} \sum_{r=1}^{R_m^\sigma} \mathbf{v}_{\sigma,r}^m \circ \mathbf{M}_{\sigma,r}^m \quad (16)$$

where  $\circ$  is the outer product operator,  $R_1^\sigma, R_2^\sigma$  and  $R_3^\sigma$  denote the number of components,  $\mathbf{v}_{\sigma,r}^1, \mathbf{v}_{\sigma,r}^2, \mathbf{v}_{\sigma,r}^3 \in \mathbb{R}^N$  are vectors along the  $x, y$ , and  $z$  axes, and  $\mathbf{M}_{\sigma,r}^1, \mathbf{M}_{\sigma,r}^2, \mathbf{M}_{\sigma,r}^3 \in \mathbb{R}^{N \times N}$  represent matrices corresponding to the  $y-z, x-z$ , and  $x-y$  planes, respectively. While for the opacity field, TensorRF-VM factorizes a 4D feature tensor, incorporating an additional mode to represent the channel dimension, which boils down to Eq. 17:

$$\mathcal{T}_c = \mathbf{B} \left[ \bigoplus_{m \in [3]} \bigoplus_{r=1}^{R_m^c} \mathbf{v}_{c,r}^m \circ \mathbf{M}_{c,r}^m \right] \quad (17)$$

where  $\bigoplus$  is the concatenation operator,  $\mathbf{v}_{c,r}^m$  and  $\mathbf{M}_{c,r}^m$  are vector and matrix factors of the opacity field, and  $\mathbf{B}$  is a feature basis matrix. After obtaining multi-channel features, we feed the feature into a shallow 3-layer MLP to yield the opacity for each item in the palette. In our experiment settings for 360° synthetic scenes, we set  $R_1^c = R_2^c = R_3^c = 48$  for opacity fields and  $R_1^\sigma = R_2^\sigma = R_3^\sigma = 16$  for density fields. The resolutions of the vector and matrix factors  $N$  are initially set to 128 and progressively increased to 300 over the training procedure. As for forward-facing scenes, we set  $R_1^c = R_2^c = 12, R_3^c = 48$  for opacity fields and  $R_1^\sigma = R_2^\sigma = 4, R_3^\sigma = 16$  for density fields. The vector and matrix factors are gradually upsampled from 128 to 640 over the training.

*Optimization.* Our training procedure follows the original TensorRF pipeline, enhanced by incorporating our proposed regularizers for palette learning and layer sparsity. Additionally, we apply a TV (total variation) loss and L1 norm penalty on the vector and matrix factors. The L1 norm weight is initially set to 8e-5 and reduced to 4e-5 after the first upsampling of the resolutions. The weight of the TV loss varies between 1, 50 depending on scene complexity. For optimization, we utilize the Adam optimizer [16] and train our models for 30,000 iterations. All experiments are conducted on a single NVIDIA RTX 3090 GPU.

## B BASELINE IMPLEMENTATIONS

In all of our baseline implementations, we reuse their officially provided code and hyper-parameters.

*NeRF + Image PCE.* In order to contrast our method with pure image-level recoloring, we employ a state-of-the-art palette-based

image color editing method [45] as the baseline. To ensure fair comparisons, we synthesize novel views using the TensorRF backbone and then utilize the original implementation provided by the authors to generate recoloring results for the scheme NeRF + Image PCE. In this original algorithm, an independent palette is calculated for each novel view. In our enhanced scheme, NeRF + Image PCE with unified palette, we modify the code to gather pixels from all training views and generate a unified palette offline prior to processing each individual view. During the editing process, colors in the target palettes are matched with the nearest colors in the edited palettes of our method.

*CLIP-NeRF + DFF.* The implementation of this baseline method is derived from [18]. Following their instructions, we extract semantic features from the training views and distill these semantics into neural fields. For the editing process, we prepare text prompts that describe our desired editing goals and optimize the scene by minimizing the distance between the embeddings of the text prompts and the embeddings of the rendered images. Additionally, we attempt to filter out rays during the optimization that do not intersect with the editing objects.

*PosterNeRF.* PosterNeRF [47] is currently implemented only on synthetic NeRF datasets, leading us to exclude its results on LLFF, NVSF, and Tank and Temples datasets. To ensure fair comparisons, we transform the camera poses from the original datasets into the coordinate systems of the PosterNeRF renderer, enabling consistent viewpoints across the experiments. For recoloring PosterNeRF, we begin by substituting the closest color in the extracted palette of PosterNeRF with the new RGB value from RecolorNeRF’s edited palette. Subsequently, we refine the palettes to achieve better results aligned with our desired editing goals.

## C EXPERIMENTS

### C.1 Ablation Study

We conduct an ablation study on the regularizers in our proposed palette learning. In the first row of Fig. 10, we disable the entire regularization on the palette learning. We can observe all the color components are over-saturated and the palette geometry is not included in the color space, i.e., unit cube  $[0, 1]^3$ . Consequently, such a palette, intended for color editing, is deemed infeasible. To address this issue, we introduced the convex hull bounding regularization  $\mathcal{L}_{hull}$ . This regularization ensures that the palette is contained within the color space. As shown in the second row of Fig. 10, the scene is successfully decomposed with the regularized palette, which leads to the success of recoloring the car. However, we find this regularizer tends to collapse the palette. In the exhibited case, the palette only consists of two editable colors, excluding the base color components in white and black, as dictated by the palette geometry. The sky-blue component of the reflection on the car window is absorbed into the white component, causing the recoloring of the reflection to fail. To overcome this issue, we further incorporate the projection-based convex regularization  $\mathcal{L}_{proj}$ , which forces colors in the palette to span a convex hull without overlapping vertices. With the addition of this regularizer, the sky-blue component is separated from the white component and forms a new vertex on the palette geometry, as shown in the last row

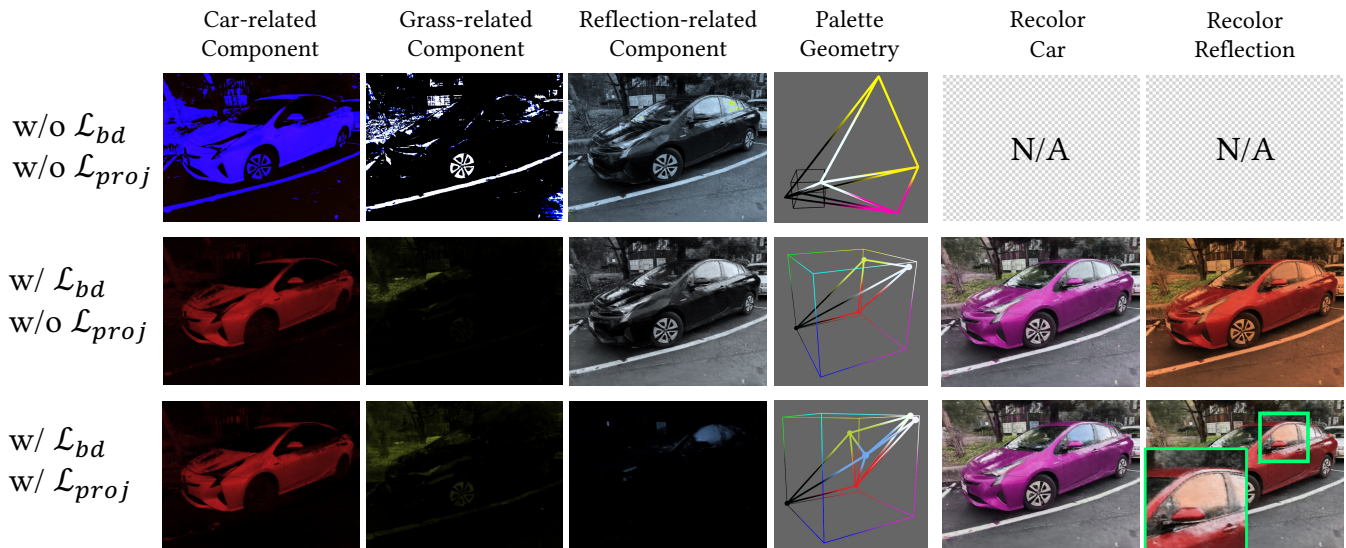


**Figure 10: Ablation study on palette learning.** In the first three columns, we visualize color components for three editing targets: car, grass, and reflection on the car window. The geometries of the optimized palettes are visualized in the fourth column, where the cubes represent the  $[0, 1]^3$  RGB space. The last two columns showcase color editing results.

of Fig. 10. This allows for a recoloring capability for changing the reflection color on the car window into “sunset red”.

## C.2 Comparisons

*Baselines.* Fig. 15 and 16 showcase more typical comparisons between our method and the baselines, which have been included in our user study for qualitative evaluation. As shown in the exhibited cases, our method outperforms the baselines on most of the complex scenes in terms of controllability and rendering quality.

*InstructPix2Pix and Instruct-NeRF2NeRF.* To highlight the advantage of our proposed palette-based color editing method, we compare the latest diffusion-based editing approaches, Instruct-Pix2Pix [4] and Instruct-NeRF2NeRF [14]. These approaches enable image-level and NeRF-level color editing, respectively. Fig. 11 presents the comparisons of our method, InstructPix2Pix, and Instruct-NeRF2NeRF. Both of the two text-guided comparison methods suffer from severe “color pollution” problems, where areas out of the editing target are significantly affected. This is due to the failure of input text prompts to precisely guide the diffusion-based generation procedure toward the intended target. In contrast, our method, which leverages palettes, enables more precise and controllable color editing.

*PaletteNeRF.* We also compare our method with the concurrent work PaletteNeRF [19]. Fig. 12 presents the recoloring comparisons on the “fern” scene. Firstly, we aimed to recolor the background lighting to “cadmium red”. It can be observed that PaletteNeRF introduces some artifacts in the lighting and shadows (Fig. 12b). In contrast, our method handles these transitional areas of lighting and shadows more smoothly and naturally (Fig. 12a). Secondly, we aimed to validate the effectiveness of our palette learning scheme, even when the palettes are randomly initialized. Our goal is to recolor the fern to red. It is worth noting that PaletteNeRF requires a time-consuming two-stage training procedure. Prior to training a PaletteNeRF, an additional vanilla NeRF model is trained to extract initial palettes, similar to the approach described in [47]. Without the pre-computed initial palette, the color editing results of PaletteNeRF degrade significantly (Fig. 12d), revealing its deficiency in palette optimization. However, our method still achieves considerable recoloring results (Fig. 12c) despite the random initialization of the palette. This is attributed to our fully learnable palettes, which are obtained jointly with radiance field optimization.

## C.3 More Visual Results

We present additional visual results in Fig. 13 and 14 to validate the effectiveness of our method, while more illustrative examples can be found in our supplementary demo videos.

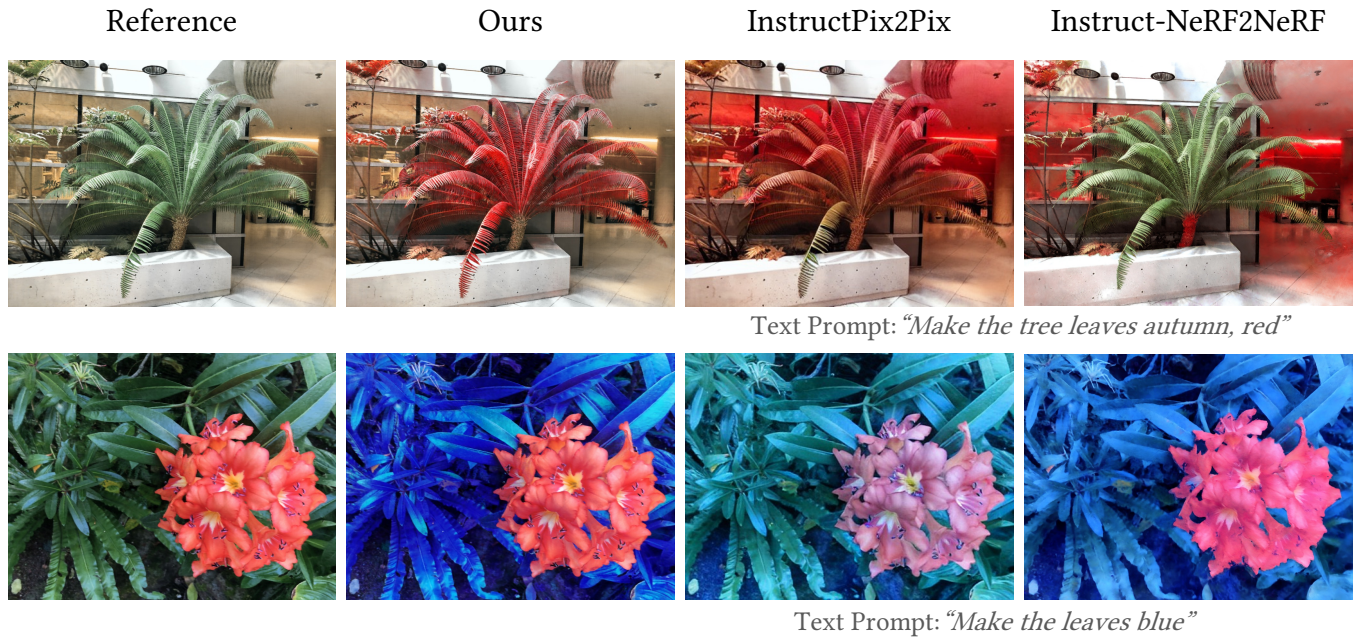


Figure 11: Comparisons of our method, InstructPix2Pix and Instruct-NeRF2NeRF. Text prompts for the two text-guided approaches are displayed below each case.

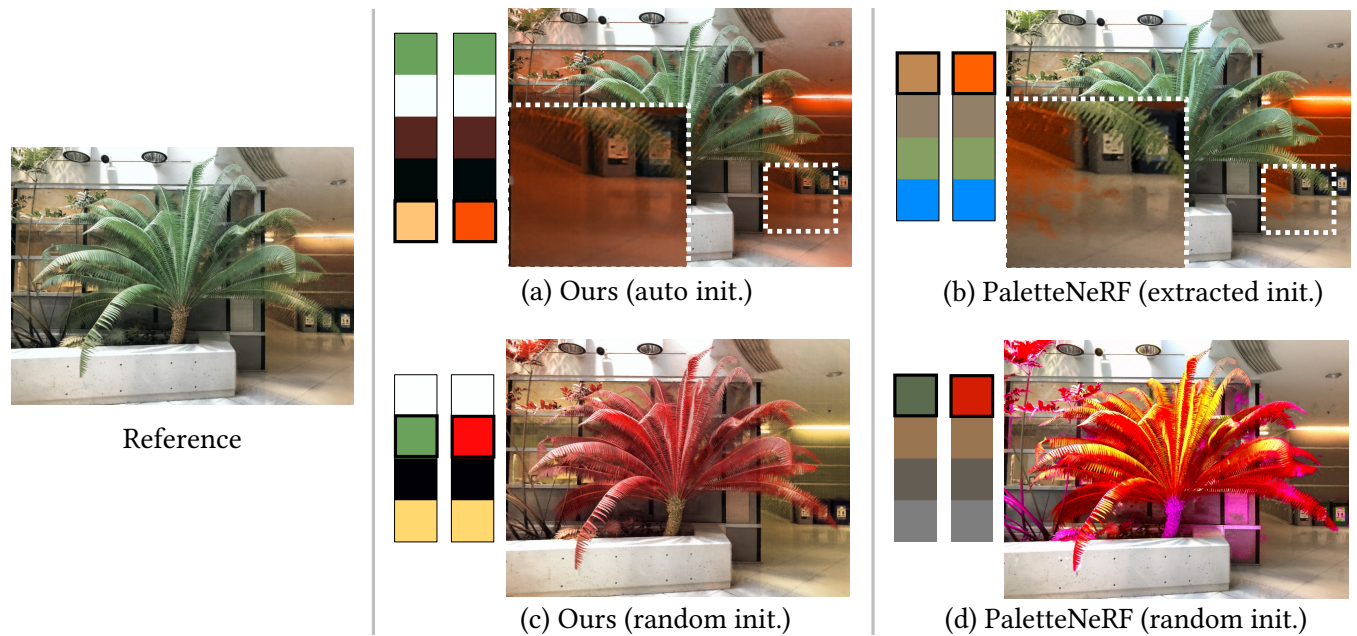


Figure 12: Comparisons of our method and PaletteNeRF. We evaluate two initialization schemes of palettes: initialization from extracted palettes (Extracted Init.) and random initialization (Random Init.).

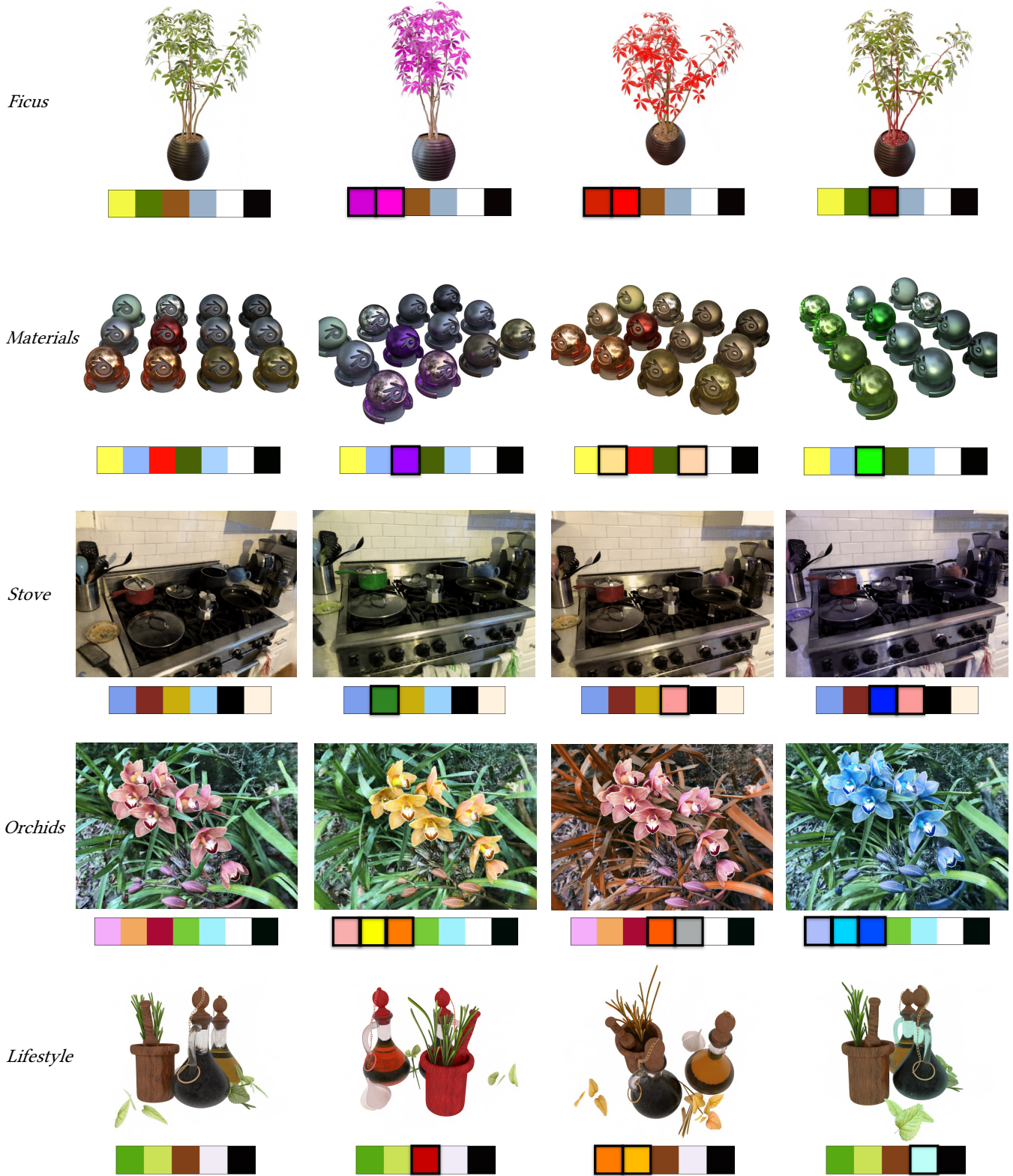


Figure 13: Gallery of our color editing results. The first image of each row is the reference before editing along with the optimized palette beneath. The other 3 images showcase 3 examples of color editing with the corresponding edited palettes.

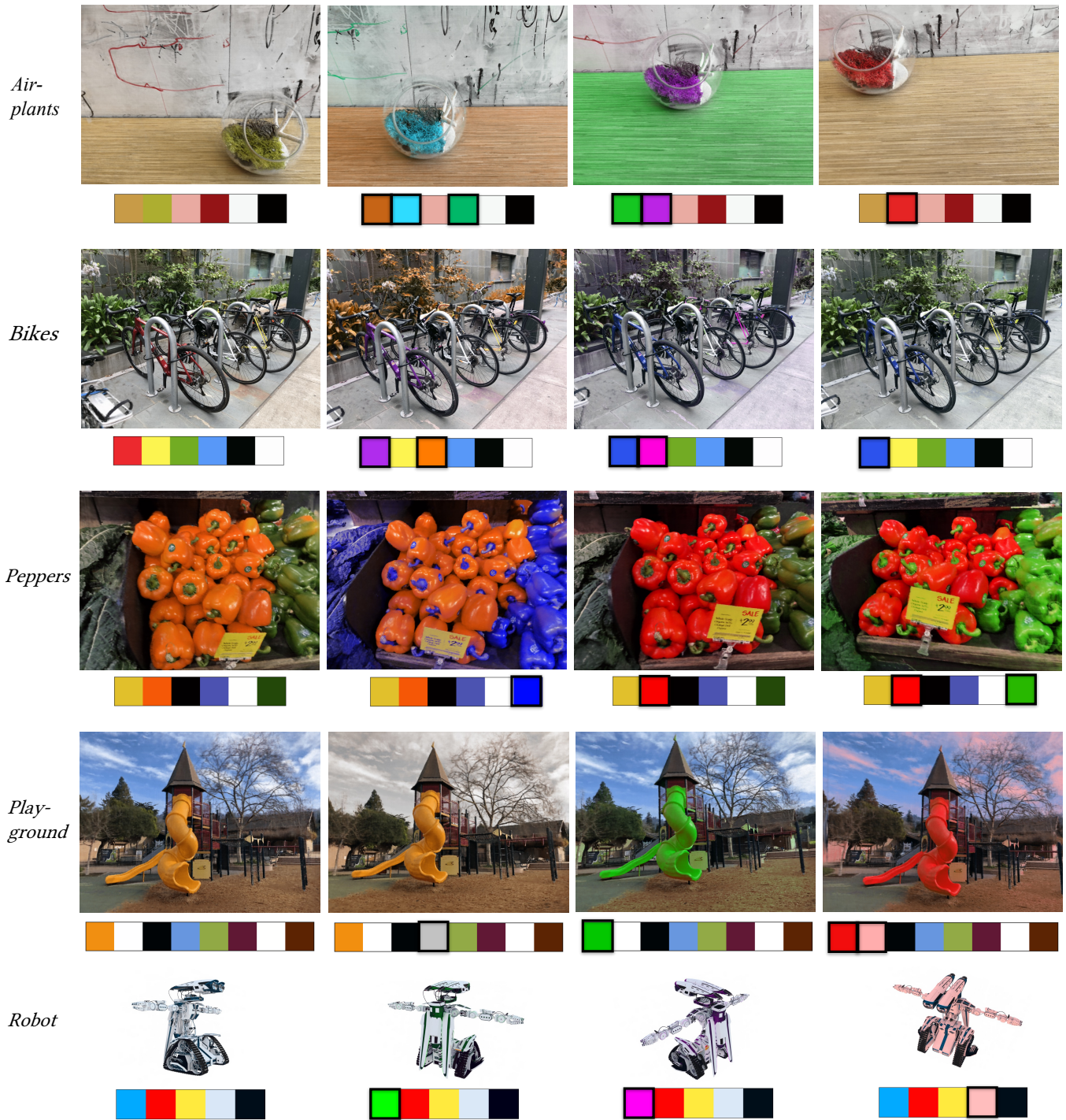


Figure 14: (cont.) Gallery of our color editing results. The first image of each row is the reference before editing along with the optimized palette beneath. The other 3 images showcase 3 examples of color editing with the corresponding edited palettes.

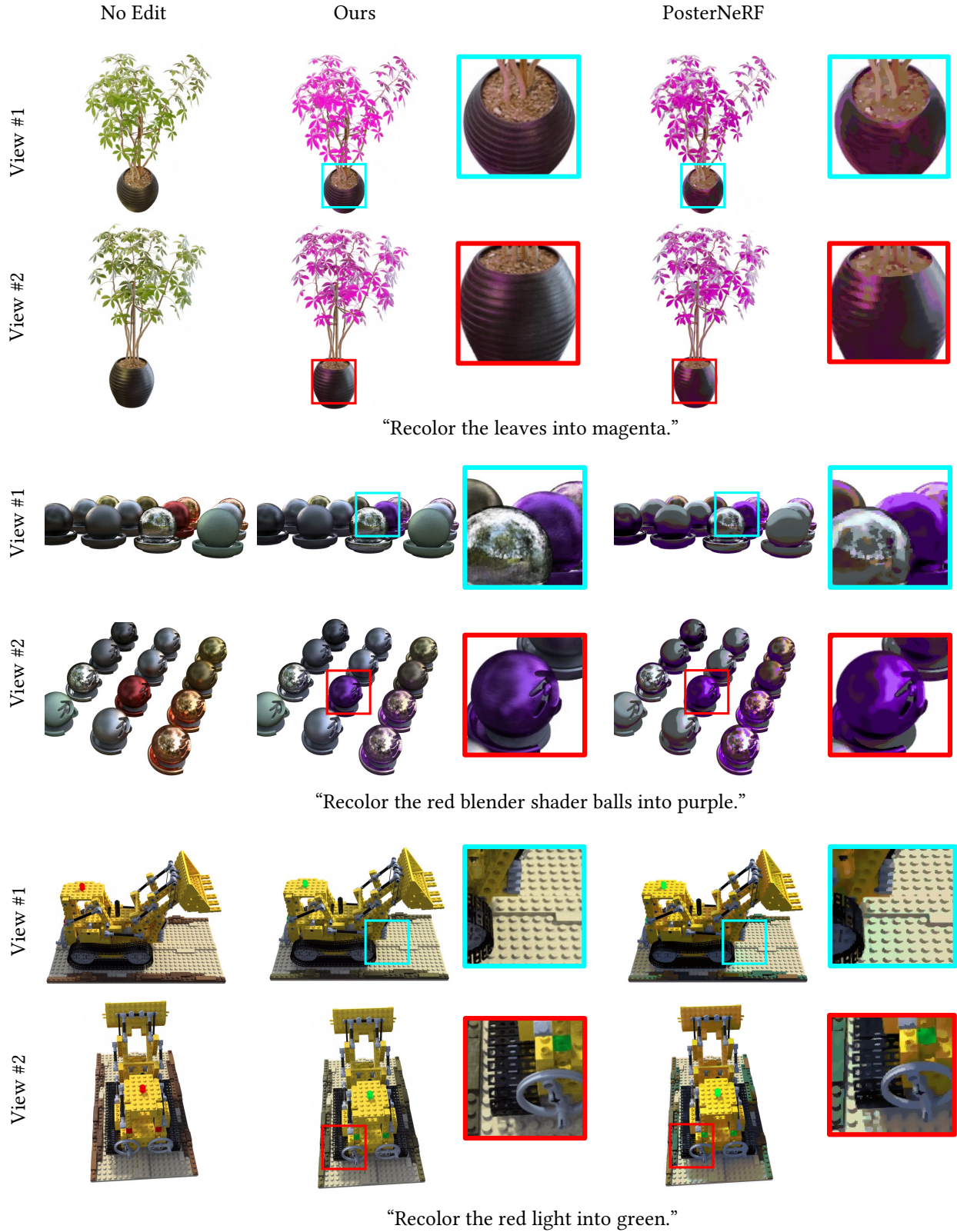


Figure 15: Comparisons of our method and PosterNeRF. Close-ups display the result details of each method. The text below each case is the desired editing goal.



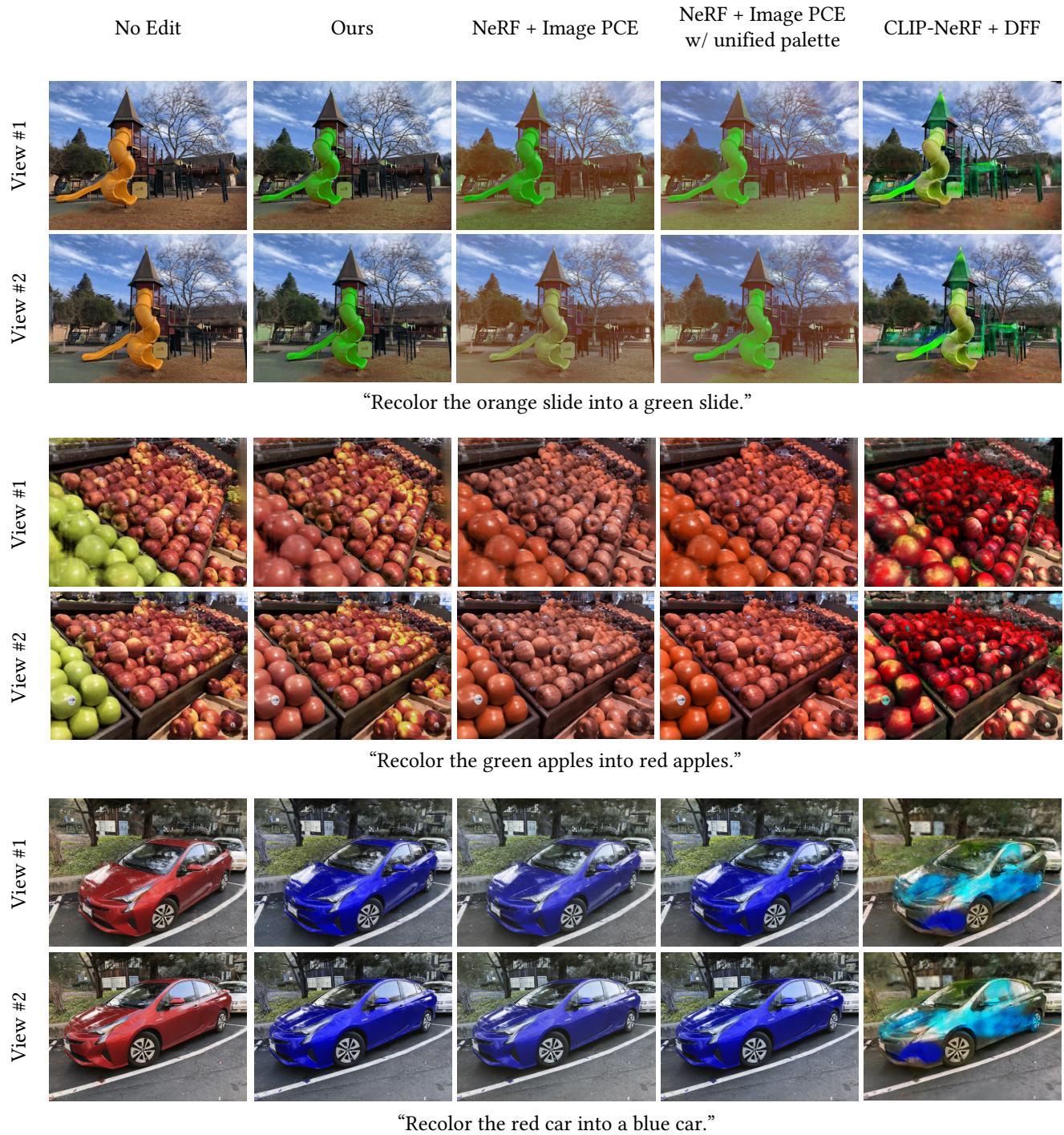


Figure 16: Comparisons of our method, NeRF + Image PCE, NeRF + Image PCE w/ unified palette, and CLIP-NeRF + DFF. The text below each case is the desired editing goal.